Power Quality and Harmonic Analysis of Multi-pulse SCR-Based Rectifiers for Industrial-Scale Water Electrolyzers Under Partial-Load Conditions

Junior Diamant Ngando Ebba[1,2], Joselyn Stephane Menye[1], Mamadou Baïlo Camara[1], Mamadou Lamine Doumbia[2], Brayima Dakyo[1], Joseph Song-Manguelle[2]

[1] *GREAH-Laboratory, University of Le Havre Normandie, 75 Rue Bellot, 76600 Le Havre, France.*

[2] *GREI-Laboratory, University of Québec à Trois-Rivieres, 3351 Bd des Forges, QC G8Z 4M3, Canada*

***Abstract*— Thyristor-based topologies are currently the most widely used for industrial-scale water electrolysis applications due to their maturity and very high current, and voltage capability for powering electrolyzers. However, several studies on these converters for supplying electrolyzers focus on power quality (PQ) analysis under nominal operating conditions. According to the literature review, load variations can accelerate the aging of electrolyzers, causing operations that reduce their lifespan, yet their impact on PQ has not been addressed. This paper proposes an analysis of PQ and harmonic issues of multi-pulse silicon controlled rectifier-based rectifiers under variables load conditions considering 12-, 18-, and 24-pulse rectifiers. This theoretical analysis aims to provide a comprehensive understanding of the effect the load's variation impact on PQ in the electrolysis process, with the goal of optimizing the design and ensuring the reliability of multi-pulse SCR-based rectifiers.**

Keywords*— *Industrial-scale water electrolyzer, Hydrogen production, Harmonic analysis, Power quality, Silicon Controlled Rectifier (SCR), multi-pulse rectifier, and Partial Loads.

I. INTRODUCTION

In recent years, the steady increase in primary energy consumption, the growth in global carbon dioxide (CO_2) emissions, and the depletion of fossil fuels have become major concern worldwide [1, 2]. This issue was further highlighted at the Paris Climate Conference, which established the goal of limiting the average global temperature increase to below 2°C above pre-industrial levels, while striving to keep the rise within 1.5°C [3]. Hydrogen, as an energy carrier produced through water electrolysis using renewable energies, offers a promising solution to reduce CO_2 emissions and meet the growing global energy demand. Figure 1 illustrates a large-scale hydrogen production system, which integrates several components that interface the electrical grid with the electrolyzer plant, including a multi-pulse transformer, a silicon-controlled rectifier (SCR), and various filtering devices. Power electronics converters play important role within the hydrogen production system, particularly ensuring the transfer of power flow between different sources (in this case, the electrical grid and the electrolyzer plant) [4]. However, their integration into hydrogen production systems introduces harmonic distortions that deteriorate power quality (PQ), causing voltage and current fluctuations likely to compromise grid stability [5]. Moreover, coupling hydrogen production with renewable energy sources, such as wind turbines or solar panels, induces power fluctuations that can lead to dynamic load variations [6]. These variations may accelerate electrolyzer degradation and, in the long term, compromise the overall stability and reliability of the system [7]. It is therefore essential to analyze the effect of load variations in order to access their impact on PQ, especially since few current studies address these issues.

M. Keddar et al. [8], presents a comparative study of 6-pulse thyristor-based and transistor-based topologies (12-pulse diode rectifier + three phases interleaved buck converter) to improve power quality for a 20 MW proton exchange membrane (PEM) electrolyzer system at Air Liquid's Bécancour Plant. Simulation results show that, compared to 6-pulse thyristor rectifier, transistor-based topology achieves a higher power factor, lower current THD (total harmonic distortion), and reduced electrolyzer current ripple, thereby lowering system costs and minimizing filter size. L. Sánchez et al. [9], present a comprehensive comparative analysis of four distinct power converter topologies (Thyristor rectifiers (TRs), diode rectifiers (DRs) with DC-DC, active front-end (AFE) power converter, and AFE power converter with DC-DC) for supplying high-power electrolyzers. The analysis covers PQ, the effects of grid voltage variations and harmonics, filtering requirements, electrolyzer aging, cost, and efficiency. Simulation results indicate that AFE and AFE+DC-DC converters provide the best performance in terms of power quality, but these topologies increase system cost and complexity. On the other hand, TR and DR+DC-DC converters exhibit lower efficiency, particularly when active filters are employed, although 6-pulse TR remains the most economical option in terms of component cost. Á. Iribarren et al. [10], proposes a new analytical model of 6- and 12-pulses thyristor rectifiers with constant-voltages loads. The model enables the analysis and optimal design of thyristor rectifiers for electrolyzers without DC-side inductance. Experimental validation using a laboratory-scale electrolyzer emulator demonstrated the accuracy of the proposed models for both 6- and 12-pulse rectifiers [10]. Z. Wang et al. [11] investigate harmonic issues in a large-scale green hydrogen plant based on a PEM electrolyzer and propose a mitigation

XXX-X-XXXX-XXXX-X/XX/$XX.00 ©20XX IEEE

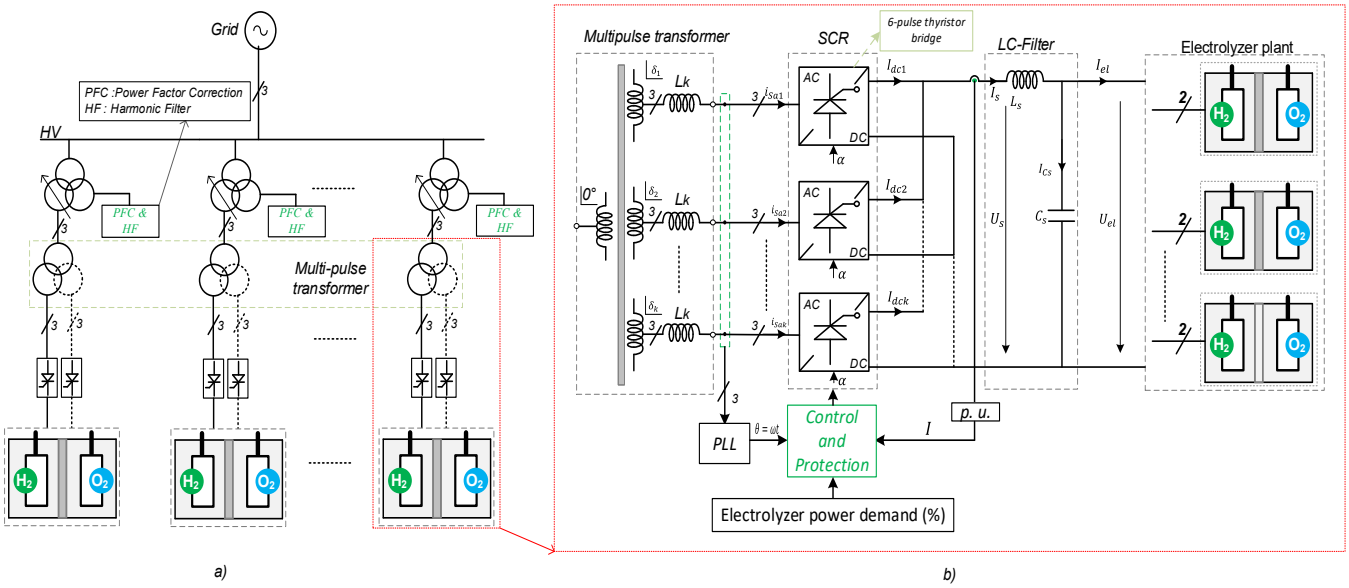

Fig. 1: Hydrogen production by water electrolysis: (a) plant configuration, (b) Electrolyzers supply configuration.

strategy combining passive and active filters for 6- and 12-pulse thyristor rectifiers. The results show that for a 6-pulse topology, a passive filter is required to suppress the 5th-order harmonic, while higher-order harmonics are mitigated by active filters. In the case of a 12-pulse topology, an 11th-order passive filter is needed, with active filters handling the higher-order harmonics (≥7). H. Hamza et al. [12] proposes an approach to scaling down electrolysis systems from the megawatt-scale to a laboratory-scale test bench by manipulating four parameters: voltage, current, cell area, and scaling factor, with a focus on energy efficiency. Three scaling approaches are considered: constant output voltage, constant output current, and constant resistance. Simulation and mathematical analysis results show that the constant voltage and constant current approaches can effectively reduce a high-power PEM electrolyzer to a laboratory configuration without compromising energy efficiency.

Several studies have investigated power quality issues and harmonic mitigation techniques, but mainly under nominal operating conditions. In this paper, we focus on industrial scale electrolyzer technologies such as alkaline and PEM electrolyzers, due to their technological maturity and high performance under dynamic operating conditions [13]. Electrolyzers require a high level of direct current (typically 5 to 25 kA) and relatively low DC voltages (a few hundred volts) [14]. For this purpose, silicon-controlled rectifiers (SCRs) represent a suitable technological choice due to their high voltage and current handling capabilities, which meet electrolyzer requirements. For instance, Infineon currently offers SCRs rated at 1.8 kV / 8.12 kA [4].

This work presents a PQ analysis of the grid side and the DC side in a large-scale hydrogen production system, where electrolyzers are supplied by SCR-based 12-, 18-, and 24-pulse rectifiers operating under variable load conditions.

This paper is organized into five sections. Section II presents the static-dynamic modeling of the 5 MW alkaline electrolyzer (AEL) considered in this study. Section III describes the different multi-pulse transformer configurations designed to provide various phase shifts for SCR-based power supplies, along with the design of the DC-side components. Section IV presents a comparative performance analysis of the investigated rectifier topologies under both rated and partial load conditions. The analysis focuses on the grid-side performance in terms of current harmonic distortion and power factor (PF), as well as the load-side performance evaluated through the ripple factor (RF). Finally, conclusions of this work are summarized in Section V.

II. ELECTROLYZER MODELING

For this study, we use a static-dynamic model of a bipolar alkaline electrolyzer. Each module has a nominal power of 5 kW (IGen 300/1/25) [15]. To achieve the desired total power, several modules are connected in series and in parallel. The effects of pressure (P) and temperature (T) are assumed to be identical across all modules.

A. Equivalent circuit model of AEL Cell.

Figure 2 illustrates a two-time-constant model of a single-cell AEL, accounting for variations in the reversible voltage $E_{\mathrm{rev},T,P}$ as a function of temperature and pressure. The series resistance and the two parallel RC networks represent, respectively, the membrane resistance (R_m), the double-layer capacitances ($C_{dl,a;}$ and $C_{dl,c}$), and the charge-transfer resistances at the anode and cathode ($R_{\mathrm{ct},a}$ and $R_{\mathrm{ct},c}$). All these parameters vary with the electrolyzer current (average and ripple current) [15].

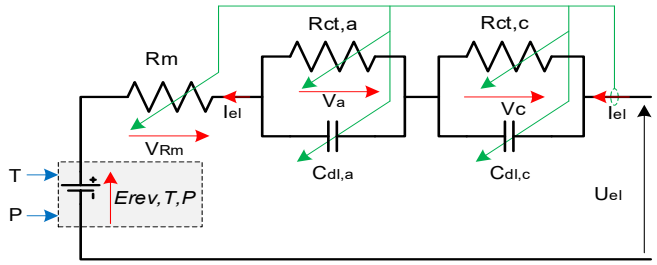

Fig. 2: Electrical circuit model (ECM) of single cell Alkaline electrolyzer.

The mathematical model of single cell AEL is defined by equation (1), where N_{Cell} is the number of cells connected in series in the stack.

$$\begin{cases} \frac{d}{dt}\begin{bmatrix} V_a \\ V_c \end{bmatrix} = \begin{bmatrix} -\frac{1}{R_{ct,a}.C_{dl,a}} & 0 \\ 0 & -\frac{1}{R_{ct,c}.C_{dl,c}} \end{bmatrix}\begin{bmatrix} V_a \\ V_c \end{bmatrix} + \begin{bmatrix} \frac{1}{C_{dl,a}} & 0 \\ \frac{1}{C_{dl,c}} & 0 \end{bmatrix}\begin{bmatrix} I_{el} \\ 0 \end{bmatrix} \\ Uel = N_{Cell}.\left(E_{Rev,T,P} + R_m.I_{el} + V_a + V_c\right) \end{cases} \quad (1)$$

The reversible voltage of the electrolyzer cell stack is defined by Eq. (2). Where, $U^0_{\mathrm{rev},T}$ denotes the reversible voltage as a function of temperature (T [°C]) at standard pressure (1 bar). The logarithmic term accounts for the effect of pressure and incorporates non-ideal operating conditions, including the vapor pressure of the KOH solution ($P_{\mathrm{v,KOH}}$) and the water activity ($a_{\mathrm{H_2O,KOH}}$). R is the universal gas constant (8.314 J/(mol.K)), z represents number of electrons transferred per mole of reaction (for water electrolysis, $z = 2$), and F is Faraday's constant (96485C/mol).

$$E_{rev,T,P} = N_{Cell}.\left(U^0_{rev,T} + \frac{R(T+237.15)}{zF} ln\left(\frac{(P-P_{v,KOH})(P-P_{v,KOH})^{1/2}}{a_{H2O,KOH}}\right)\right) \quad (2)$$

Based on the experimental results reported in [15], the data were fitted to the model shown in Fig. 2 using a nonlinear least-squares fitting algorithm, namely the Levenberg–Marquardt method, implemented in MATLAB [16]. The authors use EIS (Electrochemical Impedance Spectroscopy) characterization to build the static-dynamic behavior of 5 kW electrolyzer (at 45 °C, 25 bar). The parameters of ECM given by Eq. (3).

$$\begin{cases} R_m(I_{el}) = 0.317e^{0.007I_{el}} \\ R_{ct,a}(I_{el}) = 0.0663e^{-0.0401.I_{el}} + 0.0060 \\ C_{dl,a}(I_{el}) = -0.2347e^{-0.0389.I_{el}} + 0.6835 \\ R_{ct,c}(I_{el}) = 0.01933e^{-0.0309.I_{el}} + 0.0123 \\ C_{dl,c}(I_{el}) = 0.0333e^{-0.0226.I_{el}} + 0.0230 \end{cases} \quad (3)$$

Figure 3 shows the curves illustrating the evolution of the electrolyzer parameters obtained from experimental data and the fitting results represented by Eq. (3). Table I summarizes the different error indicators used to evaluate the accuracy between the fitted values and the experimental results. Equations (4) and (5) represent, respectively, the Root Mean Square Error (RMSE) and the coefficient of determination (R^2).

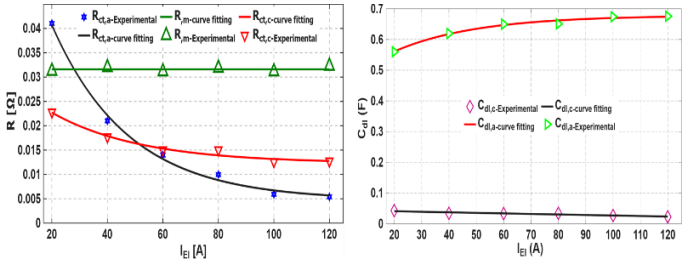

Fig. 3: Evolution of circuit parameters as a function of current: (a) Resistances, and (b) Capacitances.

$$RMSE = \sqrt{\frac{1}{N}\sum_{k=1}^{N}\left(x_{exp,i}(k) - x_{fit,i}(k)\right)^2} \quad (4)$$

$$R^2 = 1 - \frac{\sum_{k=1}^{N}\left(x_{exp,i}(k) - x_{fit,i}(k)\right)^2}{\sum_{k=1}^{N}\left(x_{exp,i}(k) - \bar{x}_{fit,i}\right)^2} \quad (5)$$

TABLE I. STATISTICAL ERROR PARAMETERS FOR NONLINEAR CURVE FIT OF PARAMETEERS.

	Parameters				
	R_m [Ω]	$R_{ct,a}$ [Ω]	$C_{dl,a}$ [F]	$R_{ct,c}$ [Ω]	$C_{dl,c}$ [F]
R^2	1.45*10^{-5}	0.9953	0.9832	0.9777	0.8742
RMSE	0.0006	0.011897	0.00723	0.00074	0.0031

B. *Polarization curve for 5MW electrolyzer.*

The 5 MW electrolyzer characteristics are illustrated in Fig. 4. To scale up this electrolyzer to 5 MW, we use multiple parallel (*Np*)-series connections(*Ns*) of 5 kW stack units. The electrolyzer parameters are regrouped in Table II.

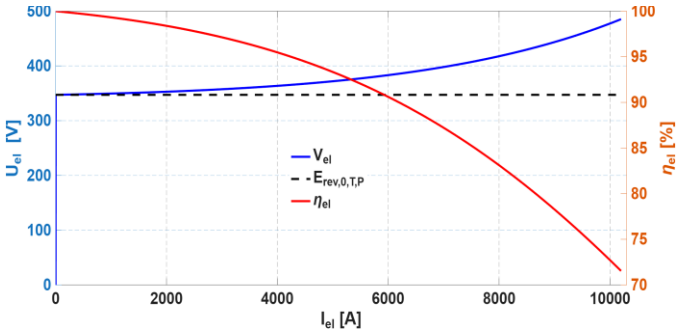

Fig. 4: I–V curve of the electrolyzer and efficiency (η_{el} (%)) at T = 65 °C and P = 25 bar.

TABLE II. ELECTROLYZER SIMULATION PARAMETERS.

P_{el} [kW]	Parameters				
	I_{el} [A]	T [°C]	N_{Cell}	P [bar]	*Stack minimum operating point [%]*
5	120	65	22	25	20-100
5000	10200		– –		

III. PHASE-SHIFTING TRANSFORMERS: PRINCIPLES AND APPLICATIONS IN MULTIPULSE RECTIFIERS.

A. *Phase-shifting transformers for multipulse SCR-rectifiers.*

The phase-shifting transformer provides three essential functions: the required phase shift between the primary and secondary line-to-line voltages in order to cancel certain harmonics, the supply of appropriate secondary voltage, and electrical isolation between the SCR-rectifier and the power supply network [17]. Two main transformer configurations can be used depending on the winding connections: a Y/Δ connection on the primary side and a Zigzag (Z) connection on the secondary side. Figure 5 illustrates a few configurations options for phase-shifting transformers used in multi-pulse rectifiers. Depending on the winding configuration, the transformer secondary line voltage can be phase-shifted relative to the primary voltage by an angle δ_i. The Y/Z-1 connection produces a leading phase shift, whereas the Y/Z-2 connection

results in a lagging phase shift. Equation. (6) represents the calculated phase shift, where p is the pulse number.

$$\delta_i(deg) = \frac{360^\circ}{p} \tag{6}$$

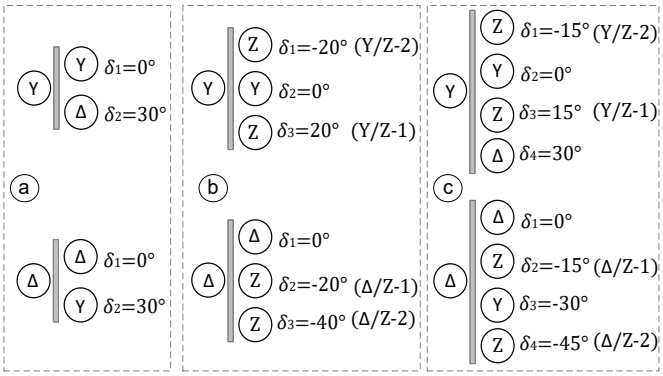

Fig. 5: A few phase-shifting transformer configurations options for multi-pulse SCR-rectifiers (a) 12-pulse, (b) 18-pulse, and (c) 24-pulse phase shifting transformer.

Figure 6 shows the typical configurations of Y/Δ, Y/Z-1, and Y/Z-2 phase-shifting transformers, along with their corresponding phasor diagrams, in which the secondary voltage V_{ab} lags the primary and secondary voltage V_{AB} by an angle δ.

The turns-ratio equations corresponding to the phase-shifting transformer configurations illustrated in Figure 6 are derived and presented in Eqs. (7), and (8) for the Y/Z-1, and Y/Z-2 topologies, respectively [17],

$$\begin{cases} \frac{N_3}{N_2+N_3} = \frac{V_Q}{V_{ax}} = \frac{\sin(30^\circ-\delta)}{\sin(30^\circ+\delta)} \\ \frac{N_1}{N_2+N_3} = \frac{V_{An}}{V_{ax}} = \frac{1}{2\sin(30^\circ+\delta)} \frac{V_{AB}}{V_{ab}} \end{cases} \tag{7}$$

$$\begin{cases} \frac{N_3}{N_2+N_3} = \frac{V_Q}{V_{ax}} = \frac{\sin(30^\circ-|\delta|)}{\sin(30^\circ+|\delta|)} \\ \frac{N_1}{N_2+N_3} = \frac{V_{An}}{V_{ax}} = \frac{1}{2\sin(30^\circ+|\delta|)} \frac{V_{AB}}{V_{ab}} \end{cases} \tag{8}$$

where N_1, N_2, and N_3represent the numbers of turns of the primary winding, the principal secondary winding, and the auxiliary secondary winding, respectively.

B. Desing of 12-, 18-, 24-pulse thyristor rectifiers.

According to Fig. 7(d), the relationship between the input and average output voltage of the 6-pulse thyristor bridge is directly related by the firing angle, as given by Eq. (9) [18]. Given that electrolyzers require a high direct current (DC) and relatively low to medium voltage levels, SCR rectifiers are connected in parallel on the DC side to increase the current supplied to the electrolyzer,

$$U_{el,avg} \approx 1.35 U_{LL} \cos(\alpha) \tag{9}$$

where $U_{el,avg}$ is the average electrolyzer voltage, U_{LL} is the line-to-line RMS input voltage, and α represent the firing angle.

1) Voltage and current ripple analysis of electrolysis power supply.

The DC current and voltage ripple represent the key parameters that affect the electrolyzer efficiency and their degradation [7]. The ripple content of the DC voltage and current is commonly quantified using the ripple factor (RF), defined as the ratio between the root mean square (RMS) value of the AC component and the average value of the corresponding DC quantity. Eqs. (10), and Eq. (11) define the voltage and current ripple factors, respectively [12].

$$RF_v(\%) = \left(\sqrt{\left(\frac{U_{el,rms}}{U_{el,avg}}\right)^2 - 1} \right) \times 100 \tag{10}$$

$$RF_i(\%) = \left(\sqrt{\left(\frac{I_{el,rms}}{I_{el,avg}}\right)^2 - 1} \right) \times 100 \tag{11}$$

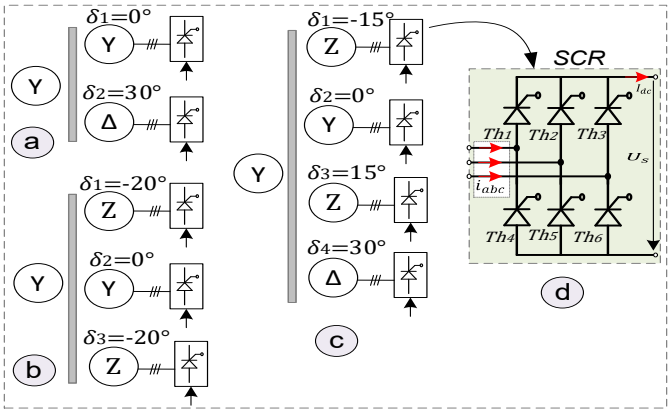

Fig. 7: A SCR-rectifiers: (a) 12-pulse, (b) 18-pulse, (c) 24-pulse, and (d) a single 6-pulse thyristor bridge representation.

2) Output LC filter design for low current and voltage ripple.

According to Fig. 1, LC-filters are designed to minimize the output ripple of the rectifier in order to meet the voltage and current ripple requirements at the electrolyzer terminals. The L_s and C_s values depend on the current and voltage ripple frequency (f_r) given by Eq. (12),

$$f_r = p \times f_g \tag{12}$$

$$L_s \approx \frac{U_{el}}{2\pi f_r \Delta I_{el}} \tag{13}$$

$$C_s \approx \frac{I_{el}}{2\pi f_r \Delta U_{el}} \tag{14}$$

where ΔU_{el} , and ΔI_{el} denote the maximum admissible voltage and current ripple at the electrolyzer terminals, respectively.

IV. SIMULATION RESULTS.

The results were obtained for $L_k = 0.05pu$ and $L_g = 0\ pu$, where $L_k$and $L_g$represent the leakage inductance and the grid line inductance, respectively. The simulation parameters used in this study are summarized in Table III.

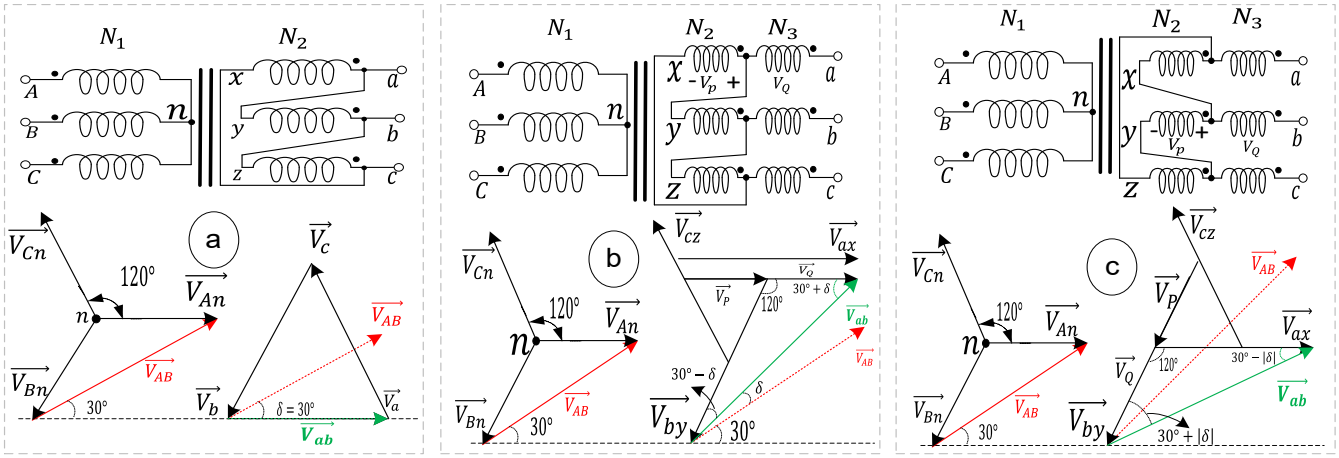

Fig. 6. Connection and phasor diagrams of (a) Y/Δ, (b) Y/Z-1 phase-shifting, and (c) Y/Z-2 phase-shifting transformers.

TABLE III. TABLE TYPE STYLES

Parameters		*Value*
Imput voltage (Grid) and frequency (f_g)		25 kV, 50 Hz
Output DC voltage		357 – 490V
Maximum output DC current		10.2 kA
Maximum current ripple (ΔU_{el})		5%
Maximum current ripple (ΔI_{el})		5%
12-pulse SCR rectifier	Ls	63.739 µH
	Cs	110400 µF
18-pulse SCR rectifier	Ls	42.493 µH
	Cs	7360 µF
24-pulse SCR rectifier	Ls	31.870 µH
	Cs	55200 µF
PI controller		Kp = 0.4305 Ki = 145

1) Close-loop results of electrolyszer power demand.

Figure 8 presents the measured power at the electrolyzer terminals ($P_{el,mes}$) in closed-loop operation along with its reference value ($P_{el,ref}$). The system is regulated using a PI controller acting on the firing angle. This figure aims to demonstrate the robustness of the controller and its ability to accurately track the imposed power reference.

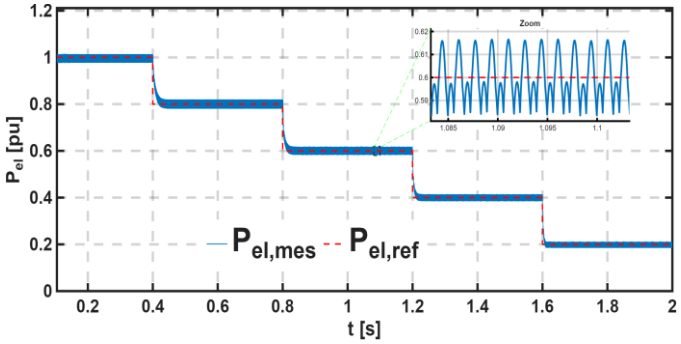

Fig. 8: Reference and measured electrolyzer power under varying load conditions.

2) Grid voltage and current measurements at nominal electrolyzer operating power.

Figures 9 and 10 respectively present the voltage and current waveforms measured on the grid side, as well as the harmonic spectra of the line current $i_{ga}(t)$ at the nominal power of the electrolyzer, together with the resulting THD.

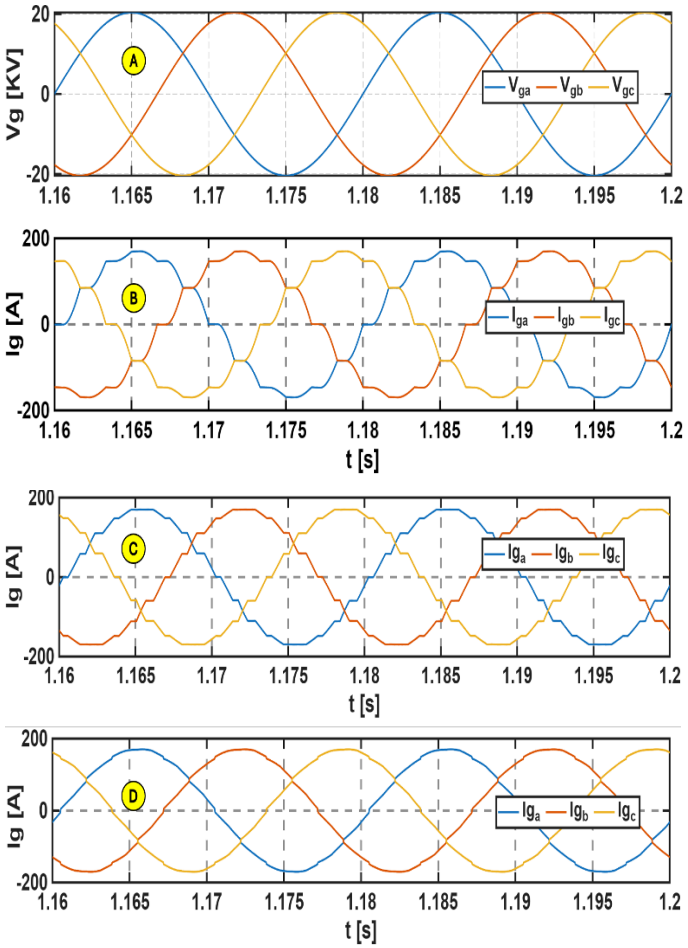

Fig. 9: Grid-side: (A) Phase-to-neutral voltage, (B) 12-pulse, (C) 18-pulse, and (D) 24-pulse grid current waveforms.

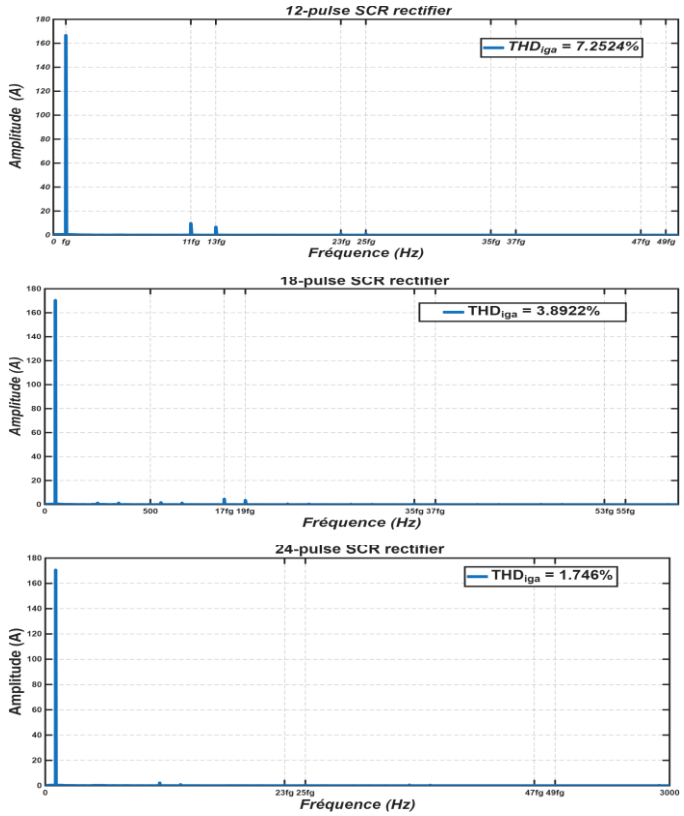

Fig. 10: Harmonic spectrum of the $i_{ga}(t)$ current waveform for the: 12-pulse, 18-pulse, and 24-pulse SCR rectifier at nominal electrolyzer power.

A comparative analysis of Figures 9A, 9B, and 9C, together with their respective harmonic spectra, shows that increasing the pulse number improves the quality of the measured current, whose waveform gradually approaches a sinusoidal shape. This improvement is confirmed by the reduction in the total harmonic distortion (THD), as illustrated in Figure 10.

3) Evolution of the THD of the grid-side current $i_{ga}(t)$ as a function of the electrolyzer partial load.

Figure. 11 illustrates the evolution of the grid-side current $i_{ga}(t)$THD as a function of the electrolyzer operating power. The results show that, regardless of the rectifier topology used (12-, 18- or 24- pulses), the THD is higher at low operating power levels and gradually decreases as the electrolyzer power demand increases.

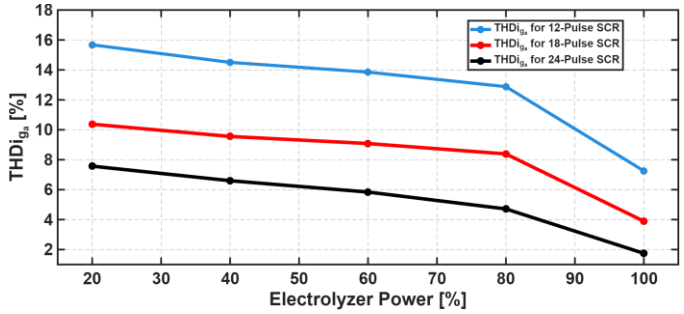

Fig. 11: THD evolution of the $i_{ga}(t)$ current waveform for the 12-, 18, and 24-pulse SCR rectifier at partial electrolyzer power.

The grid-side power factor performance under various electrolyzer operating power conditions is illustrated in Fig. 12. It can be observed that the power factor obtained with the 12-, 18-, and 24-pulse SCR converters remains nearly identical. This behavior can be explained by the fact that increasing the pulse number primarily improves the distortion factor through harmonic reduction, whereas the overall power factor is mainly governed by the thyristor firing angle (α). Consequently, regardless of the pulse number, the power factor of a thyristor-based rectifier decreases as the firing angle increases. Conversely, increasing the electrolyzer operating power leads to a reduction in the firing angle, resulting in an improvement of the grid-side power factor.

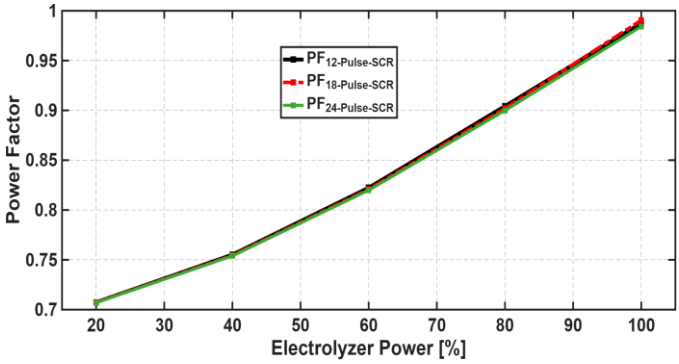

Fig. 12: Grid side power factor under various electrolyzer operating conditions.

Therefore, reactive power compensation is required to maintain a high grid-side power factor when the thyristor firing delay angle becomes significant.

4) DC-side current and Voltage ripple factor at a electrolyzer partial load evolution.

The DC current and voltage ripple factors (RF_i and RF_v, respectively), presented in Figures 1314, and 15, show that RF_v remains below 1%, Regardless of the rectifier topology considered. In addition, the RF_i varies significantly depending on the power demanded by the electrolyzer: it gradually decreases as the operating power increases.

Furthermore, the comparative analysis of the different converter topologies shows that the current ripple factor is higher for the 12-pulse topology compared with the other configurations studied.

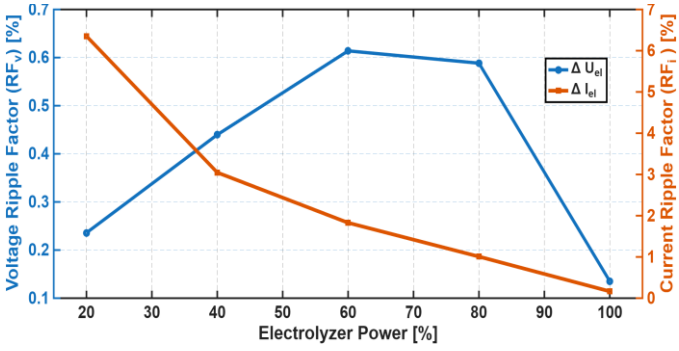

Fig. 13: DC-side Current and voltage ripple factor waveform for the 12-pulse SCR at partial electrolyzer power.

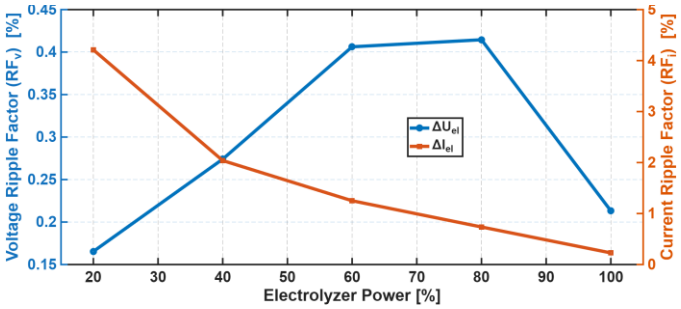

Fig. 14: DC-side Current and voltage ripple factor waveform for the 18-pulse SCR at partial electrolyzer power.

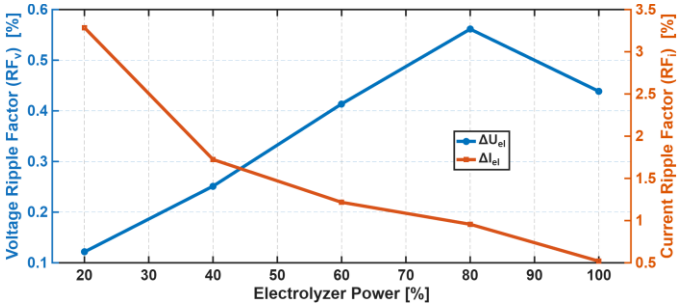

Fig. 15: DC-side Current and voltage ripple factor waveform for the 24-pulse SCR at partial electrolyzer power.

V. CONCLUSION

Hydrogen produced by water electrolysis using renewable energy sources represents a promising solution for decarbonizing major sectors (such as transportation, electricity, chemical industries) as well as for energy storage. Power electronic converters play a key role in the electrolysis process. However, their use in this system, along with operating load variations due to renewable energy, directly affects power quality and can impact the power supply network. This study aims to propose power quality analysis on 12-, 18- and 24-pulse SCR-based rectifiers under partial load operation.

The results demonstrate that the 18- and 24-pulse rectifier topologies maintain the current and voltage ripple factors within the design specifications of the LC filter over the entire electrolyzer operating range. In contrast, the 12-pulse topology exhibits a current ripple factor exceeding 5% under light-load conditions, which may accelerate electrolyzer degradation and consequently, reduce its lifespan. Furthermore, although the 18- and 24-pulse rectifiers comply with the IEEE 519-2022 current harmonic distortion limits at rated load, their harmonic performance deteriorates under partial-load conditions, making the use of harmonic filters necessary to ensure compliance with the standard. Finally, maintaining a high power factor throughout the operating range requires the integration of reactive power compensation devices, regardless of the thyristor firing angle.

ACKNOWLEDGMENT

This work is co-funded by the European Union Trough the European Regional fund (ERDF), University of Le Havre Normandie (France), and University of Quebec, Trois Rivières (Canada).

REFERENCES

[1] J. Davenport and N. Wayth, "Statistical review of world energy," *Energy institute,* 2023.
[2] H. Ritchie and P. Rosado, "Energy mix," *Our world in data,* 2020.
[3] R. Falkner, "The Paris Agreement and the new logic of international climate politics," *International Affairs,* vol. 92, no. 5, pp. 1107–1125, 2016.
[4] J. D. Ngando Ebba, M. B. Camara, M. L. Doumbia, B. Dakyo, and J. Song-Manguelle, "Industrial-Scale Renewable Hydrogen Production System: A Comprehensive Review of Power Electronics Converters and Electrical Energy Storage," *Electronics (2079-9292),* vol. 14, no. 17, 2025.
[5] B. Singh, A. Chandra, and K. Al-Haddad, *Power quality: problems and mitigation techniques*. John Wiley & Sons, 2015.
[6] X. Wang, X. Meng, G. Nie, B. Li, H. Yang, and M. He, "Optimization of hydrogen production in multi-Electrolyzer systems: A novel control strategy for enhanced renewable energy utilization and Electrolyzer lifespan," *Applied Energy,* vol. 376, p. 124299, 2024.
[7] J. D. Ngando Ebba, M. B. Camara, M. L. Doumbia, B. Dakyo, and J. Song-Manguelle, "Large-scale hydrogen production systems using marine renewable energies: State-of-the-art," *Energies,* vol. 17, no. 1, p. 130, 2023.
[8] M. Keddar, Z. Zhang, C. Periasamy, and M. Doumbia, "Comparative analysis of thyristor-based and transistor-based rectifiers for PEM water electrolysis," in *2021 12th International Renewable Energy Congress (IREC)*, 2021: IEEE, pp. 1–5.
[9] L. Sanchez, D. Reigosa, A. Bilbao, I. Pena-Gonzalez, and F. Briz, "Comparative analysis of power converter topologies for hydrogen electrolyzers," *IEEE Journal of Emerging and Selected Topics in Power Electronics,* vol. 12, no. 5, pp. 4325–4341, 2024.
[10] Á. Iribarren, E. L. Barrios, P. Sanchis, and A. Ursúa, "Modeling and Optimal Sizing of Thyristor Rectifiers for High-Power Hydrogen Electrolyzers," *IEEE Journal of Emerging and Selected Topics in Power Electronics,* 2025.
[11] Z. Wang, Y. Xu, A. Naves, A. Mabrey, and M. Lewis, "PEM-Based Green Hydrogen Plant: Harmonic Issues and Mitigation using Active and Passive Filters," in *2025 IEEE Green Technologies Conference (GreenTech)*, 2025: IEEE, pp. 21–25.
[12] H. Hamza, M. Keddar, M. Da Conceicao, M. L. Doumbia, and Z. Zhang, "Scaling Down Electrolysis System for Lab-Scale Test Bench: A Power Performance Perspective," in *2023 14th International Renewable Energy Congress (IREC)*, 2023: IEEE, pp. 1–6.
[13] A. Hassan, O. Abdel-Rahim, M. Bajaj, and I. Zaitsev, "Power electronics for green hydrogen generation with focus on methods, topologies, and comparative analysis," *Scientific reports,* vol. 14, no. 1, p. 24767, 2024.
[14] M. Tao, J. A. Azzolini, E. B. Stechel, K. E. Ayers, and T. I. Valdez, "Engineering challenges in green hydrogen production systems," *Journal of The Electrochemical Society,* vol. 169, no. 5, p. 054503, 2022.
[15] A. Ursúa and P. Sanchis, "Static–dynamic modelling of the electrical behaviour of a commercial advanced alkaline water electrolyser," *International journal of hydrogen energy,* vol. 37, no. 24, pp. 18598–18614, 2012.
[16] A. A. Fardoun, H. A. Hejase, A. Al-Marzouqi, and M. Nabag, "Electric circuit modeling of fuel cell system including compressor effect and current ripples," *International Journal of Hydrogen Energy,* vol. 42, no. 2, pp. 1558–1564, 2017.
[17] D. L. Mon-Nzongo, P. G. Ipoum-Ngome, T. Jin, and J. Song-Manguelle, "An improved topology for multipulse AC/DC converters within HVDC and VFD systems: Operation in degraded modes," *IEEE Transactions on Industrial Electronics,* vol. 65, no. 5, pp. 3646–3656, 2017.
[18] D. Guilbert and G. Vitale, "Experimental validation of an equivalent dynamic electrical model for a proton exchange membrane electrolyzer," in *2018 IEEE international conference on environment and electrical engineering and 2018 IEEE industrial and commercial power systems europe (EEEIC/I&CPS europe)*, 2018: IEEE, pp. 1–6.